Chemical Engineering Journal 299 (2016) 45–55

Contents lists available at ScienceDirect

Chemical Engineering Journal

journal homepage: www.elsevier.com/locate/cej

Green fabrication of cellulose/graphene composite in ionic liquid and its electrochemical and photothermal properties

Weijie Ye [a], Xiaoyun Li [a], Hongli Zhu [b], Xiaoying Wang [a,*], Suqing Wang [c,*], Haihui Wang [c], Runcang Sun [a]

[a] State Key Laboratory of Pulp and Paper Engineering, South China University of Technology, Guangzhou 510640, China
[b] Department of Mechanical and Industrial Engineering, Northeastern University, Boston, MA 02115, USA
[c] School of Chemistry and Chemical Engineering, South China University of Technology, Guangzhou 510640, China

HIGHLIGHTS

- Cellulose/graphene composite (CG) was obtained by exfoliating graphite in ionic liquid.
- Ionic liquid-cellulose complexes acted as exfoliating agent.
- The concentration of the obtained graphene was as high as 1.12 mg mL^{-1}.
- Carbonized CG showed desirable electrochemical performance as anode materials.
- CG was made into liquid marble as a trigger to detect the chemical reactions.

GRAPHICAL ABSTRACT

Schematic of CG preparation via direct liquid-phase exfoliation and applications as lithium ion battery anode and chemical reaction trigger.

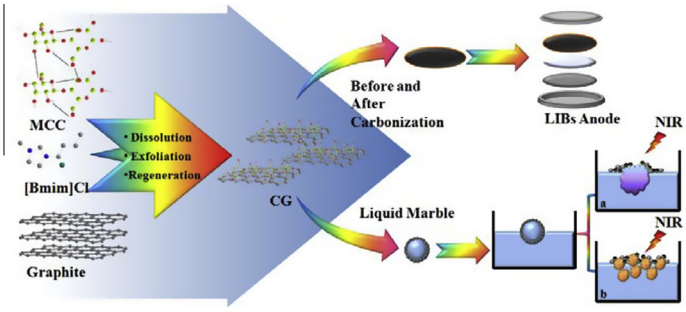

ARTICLE INFO

Article history:
Received 3 February 2016
Received in revised form 29 March 2016
Accepted 7 April 2016
Available online 16 April 2016

Keywords:
Cellulose
Graphene
Ionic liquid
Exfoliation
Lithium ion battery
Liquid marble

ABSTRACT

In this work, cellulose/graphene composite (CG) was obtained by directly exfoliating graphite in ionic liquid in presence of microcrystalline cellulose. In an ideal solvent medium provided by ionic liquid, the ionic liquid-cellulose complexes acted as exfoliating agent. The concentration of the obtained graphene was 1.12 mg mL^{-1}. The thick of graphene sheets was ~1.25 nm, and the lateral size was ~1 μm. The graphene sheets were effectively stabilized by hydrogen bonds between cellulose and graphene. Moreover, the galvanostatic charge–discharge cycling measurements of CG before and after carbonization were evaluated. Carbonization improved the initial coulombic efficiency and the cycling performance. Furthermore, the photothermal conversion study showed that CG can availably convert the near-infrared irradiation into heat, and the measured temperature reached as high as 75 °C after 1 min of irradiation. Finally, CG was made into a near-infrared-responsive liquid marble as a trigger to detect the chromogenic chemical reactions. This study provided a green method to prepare graphene nanosheets with multifunctional applications.

1. Introduction

Graphene, a 2D single layer of sp^2 carbons arranged in a hexagonal lattice, has demonstrated excellent electrical conductivity [1], outstanding thermal conductivity (5000 W m^{-1} K^{-1}) [2,3], and

* Corresponding authors. Tel./fax: +86 20 87111861 (X. Wang), +86 20 87110131 (S. Wang).
E-mail addresses: xyw@scut.edu.cn (X. Wang), cesqwang@scut.edu.cn (S. Wang).

http://dx.doi.org/10.1016/j.cej.2016.04.030
1385-8947/

admirable fracture strength (125 GPa) and Young's modulus (1100 GPa) [4]. Enjoying the desirable properties, graphene becomes a pretty promising material in many applications, such as batteries [5,6], supercapacitors [7–9], sensors [10], and semiconductor materials [11]. Owing to the excellent properties and widespread applications, an inexpensive, efficient, and green method to produce graphene with ideal structure and desirable properties has gained much attention.

Direct liquid-phase exfoliation is a convenient method to produce graphene with less oxygen functional groups, in which organic solvents, surfactants, or ionic liquids (ILs) assist to exfoliate pristine graphite [12]. However, organic solvents, such as the widely used organic exfoliation medium N-methyl-2-pyrrolidone, ortho-dichlorobenzene and chloroform, may cause toxicity [13,14]. Water-surfactant solutions comprise a simple exfoliation system, but the surfactant are hardly to remove, which may produce undesirable bubbles and have a negative effect on the subsequent application [15]. ILs are regarded as desirable green solvents for graphite exfoliation, for reasons that the high surface tension of ILs are favorable for exfoliation and the imidazolium structure of ILs can conjugate with π electrons of graphite [16–18]. However, direct liquid-phase exfoliation in ILs has serious problems, including long time for sonication and instability of the prepared graphene dispersions [19]. Therefore, an efficient liquid-phase exfoliation to produce high-quality graphene is worth studying.

As a green material, microcrystalline cellulose (MCC) is the depolymerized cellulose, which is more convenient and accessible than synthetic polymer surfactants and considered as an almost inexhaustible raw material. Moreover, owing to the large specific surface area and submicroscopic porosity, MCC exhibits an unusual affinity for hydrophobic reactants like graphite [20]. Given the plentiful hydroxyl groups in MCC, this green material may stabilize graphene sheets by forming hydrogen bonds. Notably, MCC can be dissolved well in ILs without any modification. Based on the matter mentioned above, it provides a possibility to exfoliate graphite in ILs with MCC as co-exfoliating and stabilizing agent. To our knowledge, there was no report about the use of MCC in ILs to produce graphene.

Generally, graphene obtained by direct liquid-phase exfoliation retains the intact structure and thus provides excellent electrical conductivity, but cellulose may restrict the electrical property because of inherent insulation [21]. It is noted that carbonization is a straightforward method to convert cellulosic materials into carbon [22]. The resulting carbon materials exhibit improved electrical conductivity and larger specific surface area compared with the original cellulose [23,24]. Therefore, the carbonized composite can be used as an electrode material for energy storage, such as lithium ion batteries (LIBs) or supercapacitors [5]. Additionally, graphene has attracted great interest in photothermal application because of its high light irradiation absorption and thermal conversion [25,26]. Graphene provides an important idea for preparing a controllable near-infrared (NIR)-responsive liquid marble [27,28], which is rarely reported.

Herein, we proposed a promising way to prepare graphene nanosheets and explored its various applications (Fig. 1). In the present study, cellulose/graphene composite (CG) was obtained from natural flake graphite with MCC in 1-butyl-3-methylimidazolium chloride ([Bmim]Cl) under tip ultrasonication. The effects of different graphite concentrations and MCC contents on graphene exfoliation were studied. Furthermore, the electrochemical performance of the composite before and after carbonization was studied with CG as the anode electrode. The photothermal conversion performance of CG was also investigated, and CG was further introduced into a NIR-responsive liquid marble as a chemical reaction trigger.

2. Materials and methods

2.1. Materials

Natural flake graphite was provided by XFNANO Materials Tech Co., Ltd. (Nanjing, China). MCC was supplied by Sinopharm Chemical Reagent Co., Ltd. (Shanghai, China), and its particle size was 20–100 μm. [Bmim]Cl was purchased from ChengJie Chemical Co., Ltd. (Shanghai, China) (purity, ⩾99%). Polyvinylidene fluoride (PVDF) was supplied by Micxy Reagent Co., Ltd. (Chengdu, China). Other reagents and solvents were of analytical grade.

2.2. Preparation of cellulose/graphene composite

First, 0.01 g of natural flake graphite and 0.04 g of MCC were dispersed in [Bmim]Cl followed by stirring at 110 °C for 5 h. The mixture was subjected to tip ultrasonication for 120 min (JY92-IIDN, 900 W, 2 s on, 2 s off). The resulting dispersion was centrifuged at 15,000 rpm for 10 min to remove the bulk graphite, and the supernatant containing graphene sheets was collected and retained for UV–vis test. The samples with different graphite concentrations were labeled as CG1-1, CG1-2, CG1-3, CG1-4, and CG1-5 (Table S1 in the SI). Under the same ultrasonication condition, MCC and graphite were dissolved in [Bmim]Cl separately for comparison. The ultrasonicated graphite in water, ultrasonicated graphite in IL, ultrasonicated MCC in IL, and ultrasonicated IL were labeled as UGW, UGIL, UMCC, and UIL, respectively.

Second, the mixture with different mass ratio of MCC to graphite in [Bmim]Cl was subjected to tip ultrasonication for 180 min. The resulting dispersed sample was centrifuged at 15,000 rpm for 10 min, and the supernatant containing graphene sheets in IL was collected for UV–vis test. Then, deionized water was added to initiate the regeneration. After washing the residual with deionized water, the CG samples with different mass ratio were obtained after lyophilization at −40 °C. These samples were labeled as CG2-1, CG2-2, CG2-3, CG2-4, and CG2-5 (Table S1 in the SI).

2.3. Carbonization of cellulose/graphene composite

The carbonized cellulose/graphene composite (CCG) was prepared in OTF-1200X tubular furnace (Hefei, China). The CG sample was heated from room temperature to 750 °C at the heating rate of 5 °C/min in high-purity flowing nitrogen atmosphere (50 mL/min). After carbonization at 750 °C for 2 h, the sample was cooled down to room temperature.

2.4. Characterizations

UV–vis spectra of the samples were measured with UV-1800 UV–vis spectrometer (Shimadzu, Japan). The results were the average of at least three measurements. Thermal analysis (TGA) was performed on a TGA Q500 (TA, USA). The samples were heated from room temperature to 700 °C at the heating rate of 10 °C/min in high-purity flowing nitrogen atmosphere (25 mL/min). X-ray diffraction (XRD) patterns were investigated using a D8 advance X-ray diffraction (Bruker, Germany) with a Cu Kα radiation (λ = 0.15418 nm) at 40 kV and 40 mA. Relative intensity was recorded in the scattering range of 5°–90° (2θ) at a scanning rate of 0.1 s/step. Raman spectra were obtained using the LabRAM Aramis Smart Raman Spectrometer (HORIBA Jobin Yvon, France), with He–Ne laser excitation at 632.8 nm and power at 20 mW. Fourier transform infrared (FT-IR) spectra were obtained using a Vector 33 spectrophotometer (Bruker, Germany) under a dry air atmosphere at room temperature via KBr pellets method. The

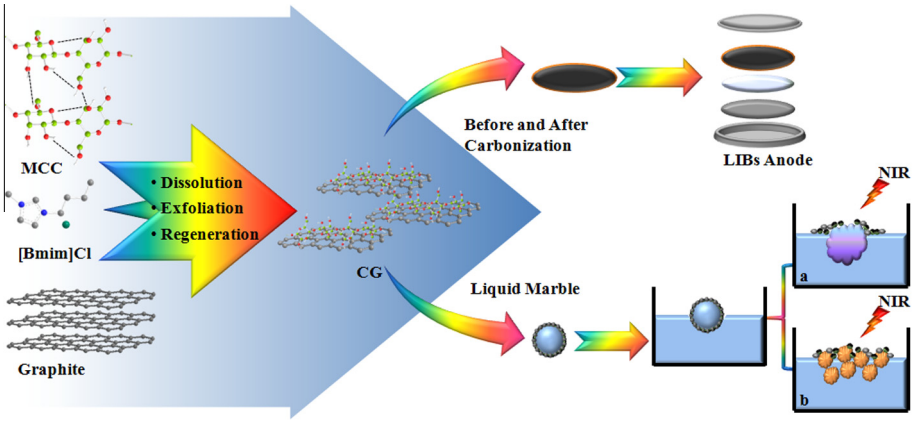

Fig. 1. Schematic of CG preparation via direct liquid-phase exfoliation and applications as lithium ion battery anode and chemical reaction trigger.

spectra were collected over the range from 4000 to 400 cm^{-1}. X-ray photoelectron spectroscopy (XPS) measurement was performed in ESCALAB 250 (Thermo-VG Scientific, USA) with a monochromatic Al Ka X-ray source (1486.6 eV). The binding energy scale was calibrated with respect to adventitious carbon (C1s).

Transmission electron microscopy (TEM) was performed using Tecnai™ G2 F30 (FEI, USA) with an accelerating voltage of 300 kV. TEM samples were dispersed in water and dropped on Cu mesh grids. Atomic force microscopy (AFM) measurement was conducted using a scanning probe microscope with Dimension Fast scan Bio (Bruker, Germany). The samples were prepared by depositing a dilute suspension on a freshly cleaved mica surface.

2.5. Electrochemical measurements

The electrochemical properties were studied in coin cells (2025). The anode slurry was prepared by mixing the active material (CG and CCG) and PVDF binder (8:2 weight ratio) in 1-methyl-2-pyrrolidinone solvent. The working electrodes were prepared by homogeneously coating the slurry on a copper foil followed by vacuum drying at 120 °C for 12 h. The coin cells were assembled in an argon-filled glove box with lithium metal as the counter electrode and by using Celgard 2325 as the separator. The electrolyte was prepared from 1 M $LiPF_6$ dissolved in ethylene carbonate–dimethyl carbonate (1:1 in volume). Galvanostatic charge–discharge cycling measurements of the assembled cells were conducted within the range of 0.01–3.00 V at 100 mA g^{-1} on the Battery Testing System (Neware Electronic Co., China).

2.6. Photothermal conversion measurements

The temperatures of UMCC, CG, PVDF, and the mixture of CG and PVDF with the weight ratio of 1:2 (CG/PVDF) were recorded by digital thermometers (UT320, China) set under the NIR irradiation (808 nm, 0.5 W) to investigate their photothermal conversion performance. All the samples were compressed into thin piece under 10 kPa.

2.7. Formation of liquid marble and its near-infrared response

CG and PVDF (1:2 weight ratio) were uniformly mixed in a vessel. A 10 μL $FeCl_3$ (0.5 M) droplet was deposited on the CG/PVDF powder bed. The liquid marble was obtained by rolling the droplet on the powder bed until the droplet was entirely encapsulated by the powder. Subsequently, the liquid marbles were separately transferred to the surface of phenol (0.5 M) and $NaHCO_3$ (0.5 M) solutions. The chemical reactions were triggered, and the liquid marble was exposed to the NIR irradiation.

3. Results and discussion

3.1. Effect of graphite concentration and cellulose content on graphene exfoliation

The UV–vis spectra of UGW, UGIL, UIL, and CG dispersions are shown in Fig. 2a. The absorption peak at 280 nm can reveal the graphene formation [29]. Compared to UGW, there is a weak absorption at 280 nm in UGIL, demonstrating an effective graphene exfoliation in IL, but IL shows no absorbance at 280 nm, thus the absorbance of the dispersions should result from the dispersed graphene. Notably, owing to the effect of MCC, the absorbance of CG were much stronger than that of UGIL, which means that the additional MCC can improve the exfoliation effect. The UV–vis spectra of CG dispersions with the fixed mass ratio of MCC/graphite (4:1) were used to investigate the effect of graphite concentration on the graphene concentration. According to the Beer–Lambert law, the absorbance is proportional to the concentration of graphite at a low concentration [30]. Therefore, the absorbance per graphite concentration (A/C_G) is used to evaluate the effect of graphite concentration on the graphene concentration. Particularly, the graphite both in the mass ratio of MCC/graphite and the graphite concentration refers to the feeding one. With increasing graphite concentration, A/C_G initially increased then decreased (Fig. 2b). When the graphite concentration was 1.43 mg mL^{-1}, A/C_G reached the maximum. The results reveal that the graphite concentration directly affected the graphene exfoliation. It can be explained that when the exfoliation proceeded at a low graphite concentration, graphite was completely dispersed in IL, a higher yield of exfoliated graphene was obtained with increasing graphite concentration. However, over the critical graphite concentration, the system was in an overcrowded state. In this case, the movement of MCC may be restrained, thereby negatively affecting the exfoliation of graphite. Consequently, A/C_G gradually decreased. Based on the above mentioned data, we propose that graphite at a concentration of 1.43 mg mL^{-1} is favorable for graphene exfoliation. Moreover, the effect of ultrasonication time (0, 40, 60, 100, and 180 min) on the graphene formation was studied (Fig. S1). The graphene concentration increased with the extension of ultrasonication time. Considering the efficiency and fragmentation issue, we selected 180 min as the proper ultrasonication time.

We subsequently investigated the effect of the mass ratio MCC/graphite on graphene exfoliation at a fixed graphite concentration of 1.43 mg mL^{-1} in 180 min. The UV–vis spectra of CG

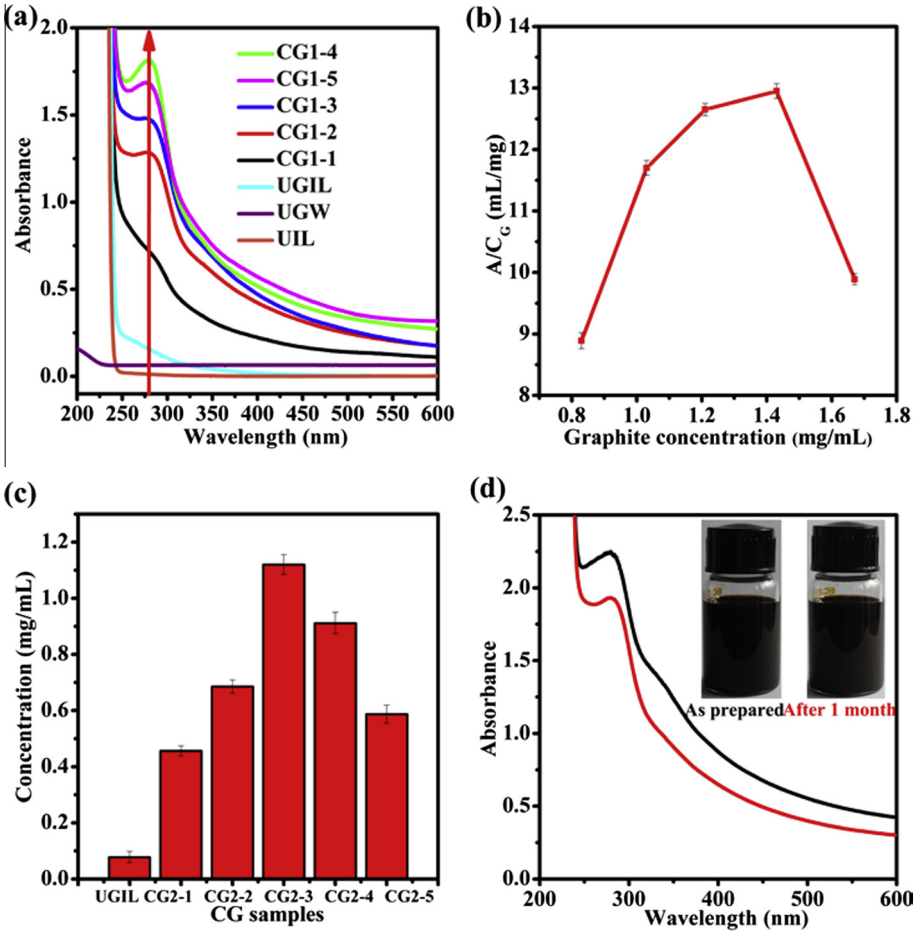

Fig. 2. (a) UV–vis spectra of UGW, UGIL, UIL, and CG dispersions with different graphite concentrations. UGW, UGIL, and UIL represent the graphite in water, graphite in IL and only IL treated with the same ultrasonication, which are used as the control group. (b) Corresponding curve of A/C_G under different graphite concentrations. The maximum A/C_G was 12.65 when the graphite concentration was 1.43 mg mL^{-1}. (c) The graphene concentration in CG with different MCC contents. When the proportion between MCC and graphite was 4:1, the CG2-3 dispersion had the maximum graphene concentration of 1.12 mg mL^{-1}. (d) UV–vis spectra of CG2-3 dispersions as prepared and 1 month later. Inset: photographs of CG dispersions as prepared and 1 month later.

dispersions with different mass ratios of MCC to graphite are shown in Fig. S2. The corresponding graphene concentration of CG is shown in Fig. 2c, which is calculated with the TG results (Fig. S3). With increasing MCC content, the graphene concentrations in CG2-1, CG2-2, CG2-3, CG2-4, and CG2-5 initially increased then decreased. High MCC content may have more interaction with graphite and accelerate the exfoliation, thus the absorbance gradually increased. However, when the MCC content was excessive, the movement of MCC was restrained, thus the exfoliation effect was weakened, and the graphene concentration gradually decreased. CG2-3 dispersion had the maximum graphene concentration of 1.12 mg mL^{-1}, which is 14 times higher than that in UGIL. Compared with the results of several reports, the resulting graphene concentration in this study is attractive. For instance, Wang et al. [31] prepared a graphene suspension (0.95 mg mL^{-1}) in 1-butyl-3-methyl-imidazolium bis(trifluoromethanesulfonyl)imide by tip sonication. Another study by Nuvoli et al. [32], a high concentration of graphene suspension (5.33 mg mL^{-1}) was obtained by bath sonication in 1-hexyl-3-methylimidazolium hexafluorophosphate, but it spent 24 h at the cost of long-time sonication involving grounding pretreatment. In addition, the UV–vis spectra of CG dispersions as prepared and 1 month later are shown in Fig. 2d. Although the absorbance decreased slightly, the resulting dark black dispersions appeared very stable, with no distinct sedimentation over a month (Fig. 2d, inset). In conclusion, we illustrated a simple method with widespread raw material and convenient process. This method can achieve a satisfactory graphene concentration and produce stable graphene in terms of liquid-phase exfoliation.

3.2. Morphology, structure and the possible formation mechanism of cellulose/graphene composite

Fig. 3a shows the AFM image of the graphene sheets. The graphene sheets are uniformly dispersed on a mica plate with lateral size of approximately 1 μm. As shown in Fig. 3b, the thickness of graphene sheet is 1.25 nm, which is corresponding to few-layer graphene [33].

The graphene sheet was also observed by TEM. A large lateral scale of graphene sheet is shown in Fig. 3c. The lateral size was up to micron scale, which is in approximation with the AFM results. The surface morphology of graphene sheets is also observed in Fig. 3d. The crinkly surface (red region) represent the folded edges of graphene sheets. Owing to the exfoliation process, the regular layer-by-layer structure is disturbed. The non-uniform interlayer arrangement of graphene sheets indicates that the layer distance of the exfoliated graphene was enlarged. Furthermore, the magnification of edge structure is shown in Fig. 3e. The distinguishable edges of the exfoliated graphene can be used to measure the layers of graphene. The layer outline indicates that the obtained graphene exhibited a few layers, which is corresponding to the AFM results. A 2D honeycomb lattice structure could also be

observed in Fig. 3f. The regular arrangement of carbon demonstrates that CG retained the relatively intact structure of graphene after exfoliation. The selected area of electron diffraction image (Fig. 3f, inset) is a proof of the typical hexagonal crystal structure of graphene.

XRD patterns of graphite, UGIL, MCC, UMCC, and CG are shown in Fig. 4a. Typically, graphite exhibits a characteristic sharp peak (002) at 26°, which is corresponding to its high crystallization. However, the (002) peak of UGIL decreased greatly, revealing the crystallinity of graphite was decreased to a certain degree with ultrasonication. Compared with MCC, UMCC presents a nearly smooth line owing to the decrease of crystallinity and the depolymerization with dissolution and ultrasonication [34]. In addition, all the (002) peaks in CG are much lower than that of graphite and UGIL, which corresponds with the graphene sheet reported by Lee and co-workers [35]. Consequently, it is further confirmed that MCC worked as an exfoliating agent in graphene exfoliation.

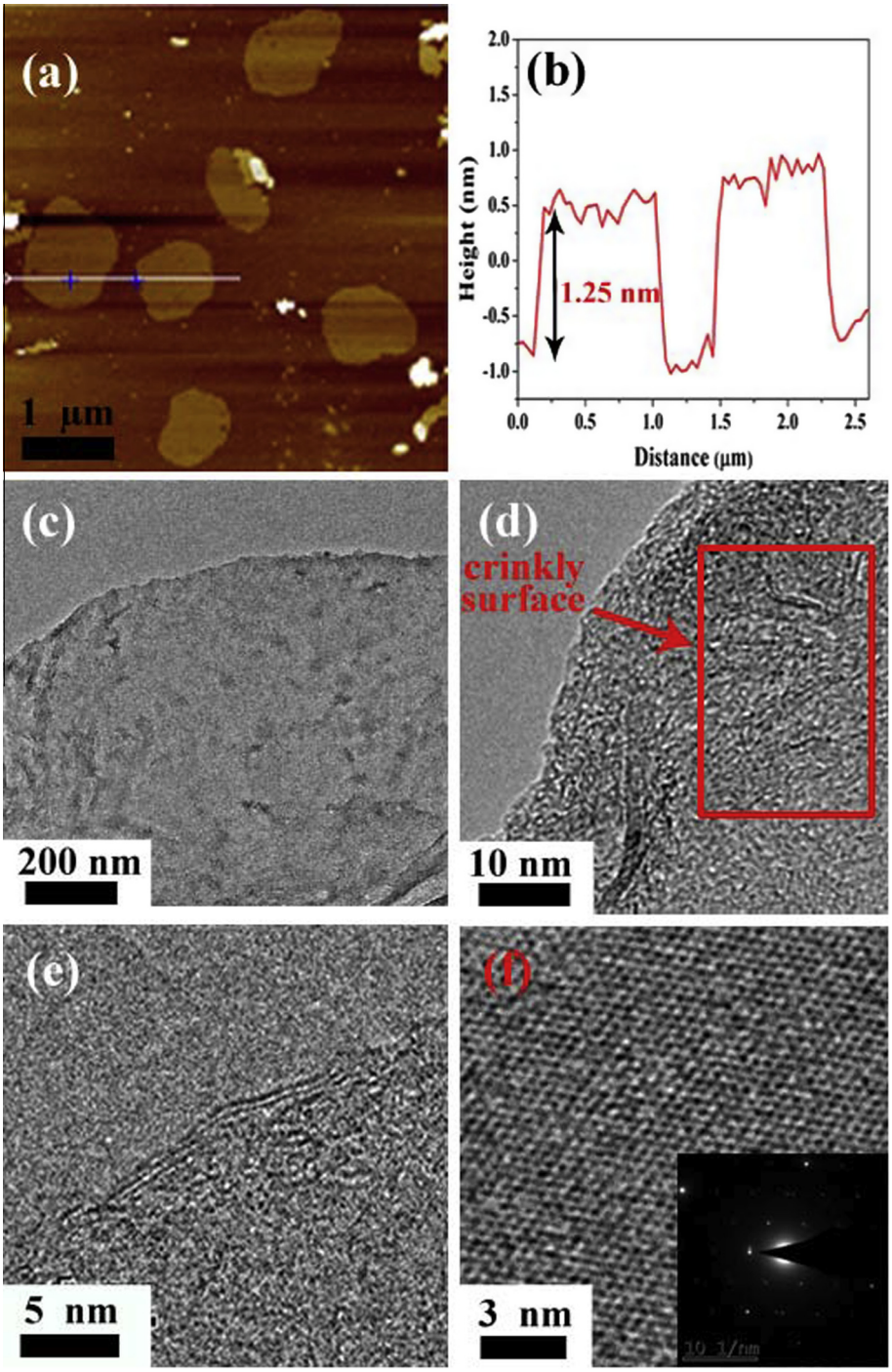

Fig. 3. (a) AFM image of graphene sheets and (b) corresponding height profile illustrates that the graphene sheets are 1.25 nm thick with lateral sizes of approximately 1 μm. TEM images of graphene sheets with different features: (c) the graphene sheet plane shows that the lateral size is up to micron scale, (d) the crinkly surface (red region) confirms the successful exfoliation, and (e) the edge of the graphene sheet presents a few-layer structure, (f) HRTEM image of graphene and the corresponding selected area electron diffraction image (inset) reveal the hexagonal structure of graphene. (For interpretation of the references to color in this figure legend, the reader is referred to the web version of this article.)

Raman spectra of graphite and CG are shown in Fig. 4b. The pronounced D peak, G peak, and 2D peak appeared at 1330, 1573, and 2676 cm^{-1}, respectively. D peak was the A_{1g} breathing pattern on behalf of sp^3 hybridized carbons. G peak was the E_{2g} vibration mode on behalf of the carbon ring or the stretching movement of sp^2 carbons. The 2D peak was attributed to a couple of phonons with opposite momentum in the double-resonance Raman process [36]. In the Raman spectra of CG samples, the enhanced 2D peaks and the slight red shift confirmed the formation of graphene [37]. Moreover, the intensity ratio of D peak to G peak (I_D/I_G) is a measure for the disorder degree of carbon materials, and an increased ratio represents the increase of edge structure [37]. The calculated I_D/I_G values of graphite and different CG samples were 0.096, 0.183, 0.149, 0.102, 0.194, and 0.201, respectively. The I_D/I_G values of CG were much smaller than those of reduced graphene oxide, indicating that the composites contained less defects and retained a relative intact structure [38]. When blocky graphite was exfoliated into graphene fragments, the cellulose molecule can be rearranged along the graphene surface, thus forming a 3D network structure during regeneration. With the increase of MCC content, the I_D/I_G initially decreased then increased. It can be explained that the certain increase of MCC content can promote exfoliation and protect graphene fragments from further abruption, thereby decreasing the edge structures. However, when MCC content became excessive, the exfoliation effect was weakened and the sizes of graphene sheets probably decreased, which means more presence of edge structures. The result is in agreement with the analysis in Fig. 2.

FT-IR spectra of MCC, graphite, UMCC, and CG2-3 are shown in Fig. 4c. For MCC, the broad absorption band centered at 3340 cm^{-1} can be ascribed to the stretching vibration of O—H arising from the hydroxyl groups. The peak at 2893 cm^{-1} referred to the saturated C—H stretching vibration, whereas the peak at 1445 cm^{-1} referred to the C—H bending vibration. The peaks at 1030, 1060, 1114, and 1164 cm^{-1} corresponded to the C—O stretching vibrations of C6H2—O6H, C3—O3H, C2—O2H, and C1—O—C4 [39]. After ultrasonication, the absorption peak of hydroxyl groups slightly shifted to 3427 cm^{-1} in the spectrum of UMCC because of the fracture of hydrogen bonds [40]. In addition, the absorption peak at 2893, 1030, 1060, 1114, and 1164 cm^{-1} weakened in the spectrum of UMCC, which was considered to be the rupture and dehydration of cellulose [41]. Another peak at 761 cm^{-1} was attributed to the olefin C—H bending vibration. The absorption peaks at 1640 cm^{-1} were ascribed to absorbed water. For CG2-3, the spectrum retained the main character of graphite except the C—O stretching vibration at 1030 cm^{-1} and the saturated C—H stretching vibration at 2893 cm^{-1}, which belonged to UMCC, indicating that the CG2-3 consisted of UMCC and graphene. Moreover, CG2-3 possessed a larger full width at half maximum at 3427 cm^{-1} compared with graphite, which was mainly ascribed to the hydrogen bonds between graphene and cellulose molecule. Besides, the slight absorption peaks at 1156 cm^{-1} of UMCC and CG2-3 were ascribed to the C—N bond [42], which were largely due to the residual [Bmim]Cl.

Fig. 5 shows the survey XPS spectra of graphite, MCC, UMCC, and CG2-3 along with the C1s high resolution XPS spectra of MCC, UMCC, and CG2-3. In Fig. 5a, the oxygen content in UMCC clearly decreased compared with that in MCC, owing to the dehydration during ultrasonication, which is in agreement with the FT-IR results. In addition, the survey XPS spectrum of CG2-3 mainly consisted of the O1s and C1s peaks because of the components of MCC and graphene. The spectral deconvolution of the C1s high resolution XPS spectrum for MCC are shown in Fig. 5b. The corresponding binding energies of 284.7, 286.3, and 288.6 eV were

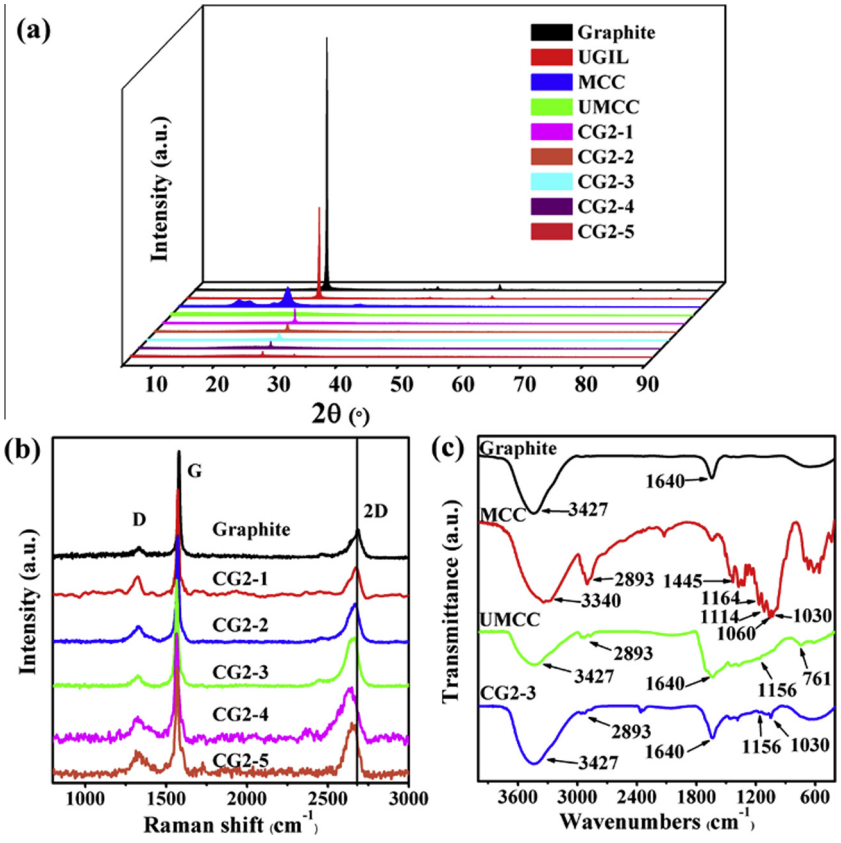

Fig. 4. (a) XRD patterns of graphite, UGIL, MCC, UMCC, and CG. Comparing with graphite or UG, the decreased crystallinity of CG demonstrates successful exfoliation. (b) Raman spectra of graphite and CG. The red shift and increasing intensity of 2D peak in CG represent the decrease of graphene layers. (c) FT-IR spectra of graphite, MCC, UMCC (with less oxygen-containing structure), and CG2-3 (with combining characteristic structures of MCC and graphite).

attributed to C—C, C—O, and O—C—O, respectively [43]. Compared with the C1s high resolution XPS spectrum of MCC, the relative peak intensity of C—O and O—C—O in UMCC decreased accordingly (Fig. 5c), which also indicated the decrease of oxygen content. The C1s high resolution XPS spectrum of CG2-3 in Fig. 5d revealed the existence of four types of carbons: C—C (284.7 eV), C—N (285.4 eV), C—O (286.3 eV), and O—C—O (288.6 eV). The C—C peak was generated by graphite and carbons in aliphatic hydrocarbon [44]. The C—O and O—C—O peaks belonged to MCC. It is noted that the spectra of UMCC and CG2-3 both presented the C—N peak, which was attributed to the imidazolium structure from the IL [45]. The presence of nitrogen indicated that the residual IL adsorbed on the samples. As a powerful solvent, IL provided an ideal medium and acted as a co-exfoliating agent for the exfoliation by the strong non-covalent interactions with graphene and cellulose molecule, which was unable to remove completely [46]. The results show that the C1s peaks of CG2-3 had no obvious changes or shift and displayed the characteristic peaks of UMCC and graphite, demonstrating that this method hardly introduced any chemical reaction on graphene sheets.

Based on the above results, the proposed formation mechanism of CG is shown in Fig. 6. First, the intra- and inter-molecular hydrogen bonds in MCC were broken up during dissolution in IL. Simultaneously, solvate complexes were formed by the new bonds between hydrogen atoms of hydroxyl in the MCC molecule and the chloride in [Bmim]Cl [47]. Van der Waals forces in the graphite interlayers were weakened in IL because of the conjugation between π electron and imidazolium. Second, through ultrasonication, the expanded bubbles carrying the potential energy were converted into the liquid jet with kinetic energy. The liquid jet then penetrated the bubbles and hit the graphite and MCC molecule [48]. In the subsequent exfoliation step, owing to the decrease in van der Waals forces between the graphite interlayers in IL, the solvate complexes containing MCC molecules exfoliated the graphite into graphene under the influence of the liquid jet and bubbles. Most importantly, MCC molecule can provide hydroxyl groups to form hydrogen bonds with π electron, thereby further decreasing the van der Waals forces between the graphite interlayers [19,49,50]. Afterward, the solvate complexes entered the graphite interlayers. Finally, the intra- and inter-molecular hydrogen bonds of MCC were reformed. As a stabilizing agent, MCC was regenerated on the graphene surface during the regeneration process. Consequently, the obtained graphene layers were stabilized effectively.

3.3. Electrochemical properties

CG and CCG electrodes were used as lithium ion batteries anodes to evaluate the electrochemical properties. Fig. 7 shows the charge and discharge curves, the cycling performance, and the coulombic efficiencies at a current density of 100 mA g^{-1} between 0.01 and 3.00 V. The first discharge and charge capacities are 1804 and 644 mAh g^{-1} for CG (Fig. 7a), and the following four cycles were nearly similar (408 mAh g^{-1} in the fifth cycle). Owing to the introduction of MCC molecule, the graphene sheets can maintain a stable state. But the hydroxyl groups of MCC may attract the lithium ions via electrostatic interaction. Hence, the transfer of lithium ion may be blocked. Besides, the conductivity is weakened because of the insulation of MCC. So the capacities diminish significantly in the subsequent cycles.

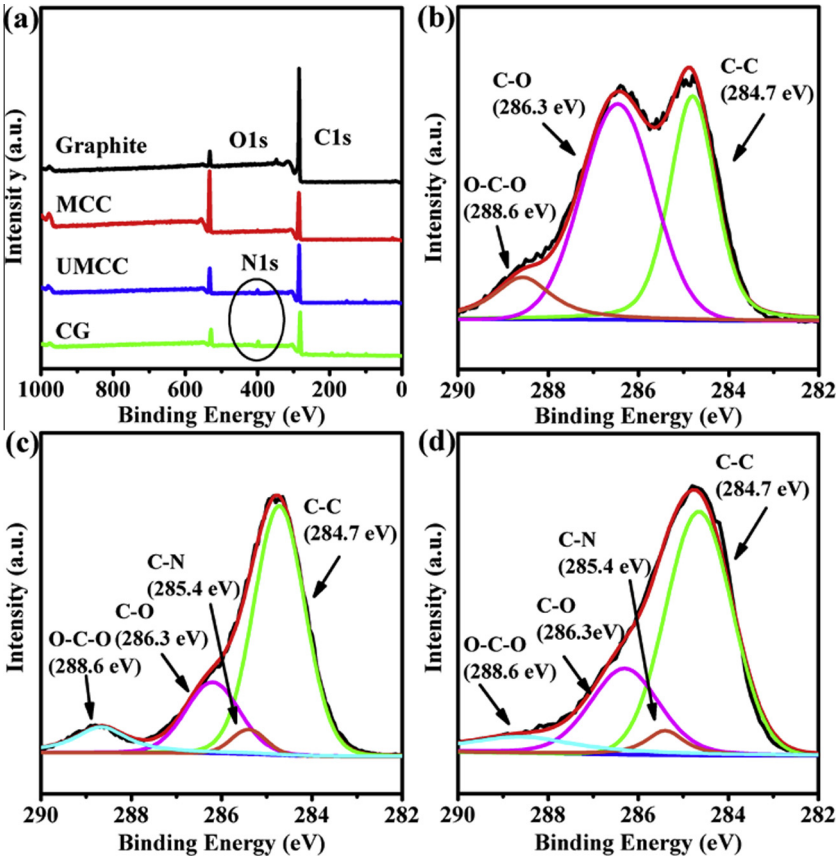

Fig. 5. (a) Survey XPS spectra of graphite, MCC, UMCC, and CG2-3. The corresponding atomic ratios for C1s to O1s are 10.42, 1.88, 4.15, and 10.32. C1s high resolution XPS spectra of (b) MCC, (c) UMCC, and (d) CG2-3 demonstrate that C1s for MCC vary after ultrasonication and CG is composed of graphene and UMCC.

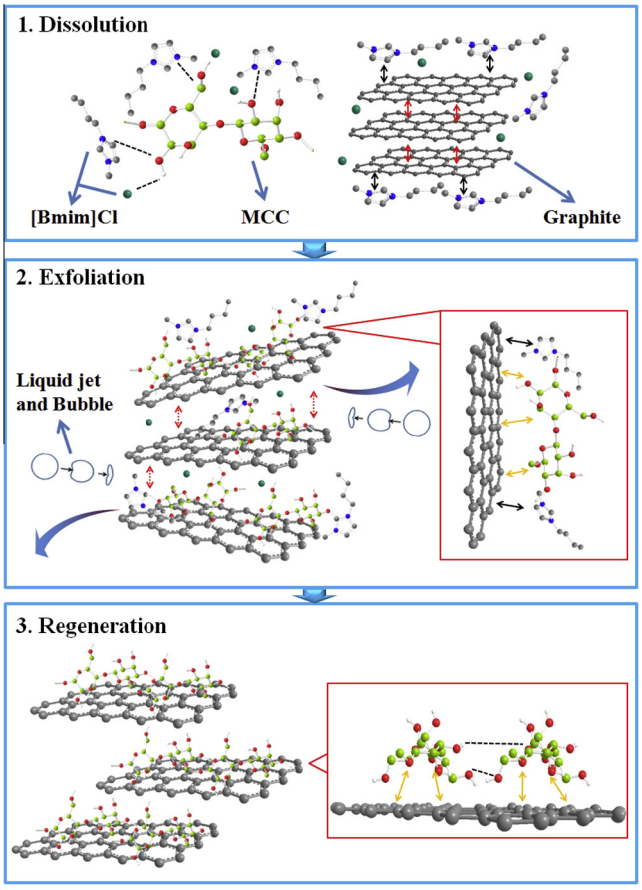

Fig. 6. Schematic formation course of CG obtained from MCC and graphite in IL under ultrasonication. (1) MCC dissolved in IL. Solvate complexes were formed by hydrogen bonds between MCC and IL. Graphite dispersed in IL. Van der Waals forces (red arrows) between graphite interlayers decreased owing to the conjugation with IL (black arrows). (2) In the presence of the solvate complexes, the van der Waals forces further decreased because of the affinity of MCC and graphite (yellow arrows). Under the influence of liquid jet and bubbles, graphene was exfoliated with the assistance of solvate complexes. (3) During regeneration, IL was replaced by water, and hydrogen bonds in MCC were formed, resulting in CG formation. The obtained graphene layers were stabilized effectively by MCC. (For interpretation of the references to colour in this figure legend, the reader is referred to the web version of this article.)

To enhance the electrical property, CG was carbonized to obtain CCG. For CCG (Fig. 7b), the first discharge and charge capacities of CCG are 1280 and 570 mAh g^{-1} and the fifth cycle nearly reached 558 mAh g^{-1}. The initial discharge capacity of CCG was lower than that of CG. This is because the process of carbonization may result in the loss of hydroxyl groups of MCC. But compared with CG in the later cycles, CCG not only showed improvement of the discharge and charge capacities but also demonstrated a better cycling performance. The reasonable explanation is that MCC was transformed into graphite-like material after carbonization, which is favorable for electrical conductivity. Nevertheless, CCG showed a better electrochemical performance than the graphene obtained by oxidation–reduction reaction and the traditional graphite anode material in LIBs [51,52].

The cycling performances of CG and CCG are shown in Fig. 7c and d. The irreversible capacity of CG reached 1160 mAh g^{-1}, whereas that of CCG was only 710 mAh g^{-1}. Along with the increase of cycle numbers, the discharge capacity of CG was 328 mAh g^{-1} with the capacity retention rate of 48.2% after 50 cycles, whereas the discharge capacity of CCG was 685 mAh g^{-1} with the capacity retention rate of over 90% after 50 cycles. These results illustrate that the carbonization treatment enhanced the cycling performance. Additionally, Fig. 7c and d also show the coulombic efficiencies of CG and CCG. A higher coulombic efficiency indicated a larger utilization capacity. Notably, the first coulombic efficiency of CG was only 35.7%, whereas that of CCG is 44.5%. In particular, at the 50th cycle, the coulombic efficiency of CG reached 97.9%, whereas that of CCG was as high as 98.3%. It can be explained that the high-temperature thermal treatment removes the functional groups in MCC, so the reaction between functional groups and electrolyte is restrained, and the irreversible capacity of CCG decreased. Moreover, owing to the carbonization process, CCG processed better electrical conductivity and provided the conductive path among graphene sheets and more active sites to transfer lithium ions. Therefore, a stable intercalation and de-intercalation process of lithium ion was established and the cycling performance was enhanced with carbonization.

3.4. Photothermal conversion

The photothermal investigation of UMCC, PVDF, CG, and CG/PVDF is shown in Fig. 8a. The steady temperature of UMCC was at about 30 °C after 1 min of NIR irradiation, which illustrates that UMCC exhibits no photothermal property. Notably, for CG, the temperature increased rapidly and reached 75 °C after 1 min because of the excellent photothermal property of graphene. With the addition of PVDF, the temperature decreased to 62 °C because PVDF also lacked photothermal property. Therefore, by efficiently converting NIR light energy into heat, CG can be a potential candidate in photothermal application.

For further investigation, the NIR-responsive liquid marble was formed using CG/PVDF as the outer shell. The liquid marble formation and triggered mechanism are shown in Fig. 8b. Different from the conventional liquid marble wrapped with hydrophobic powders, the CG/PVDF liquid marble was comprised of the hydrophobic graphene and the hydrophilic cellulose. The existence of cellulose can enhance the interaction between the powders and liquid, so as to increase the loading on the liquid surface. Besides, PVDF was used as binder to connect CG. When the liquid marble was exposed to NIR irradiation, the graphene converted NIR energy into heat. Once the inner liquid was heated to expand, the liquid marble burst and the liquid came out. The liquid marble can even move on a liquid surface and then was split by NIR irradiation, as shown in the Supplementary video. Two examples of NIR-triggered chemical reactions are presented in Fig. 8c and d. First, a liquid marble containing $FeCl_3$ (0.5 M) floated on the surface of phenol solution (0.5 M). The color changed from colorless to purple as soon as the liquid marble was triggered to burst by NIR irradiation. This typical chromogenic reaction between phenol and iron trichloride could identify the enol structure. Second, a liquid marble containing $FeCl_3$ (0.5 M) floated on the surface of $NaHCO_3$ solution (0.5 M). After NIR irradiation, the $Fe(OH)_3$ and CO_2 were generated, which reveals that the reaction was successfully triggered by NIR irradiation. Generally, the double hydrolytic reactions were created by weak acid anion and weak alkali cation and may generate precipitation, as well as a large amount of bubbles. In conclusion, the two reactions could be triggered after NIR irradiation, and the reaction formulas were described as follows:

$$C_6H_5\text{-}OH + FeCl_3 \rightarrow H_3[Fe(C_6H_5O)_6] + 3HCl$$

$$NaHCO_3 + FeCl_3 \rightarrow Fe(OH)_3 \downarrow + NaCl + CO_2 \uparrow$$

Predictably, the NIR-responsive liquid marble made of CG/PVDF can also be developed to detect other chemicals with characteristic reactions, especially the explosive and toxic agents in severe conditions.

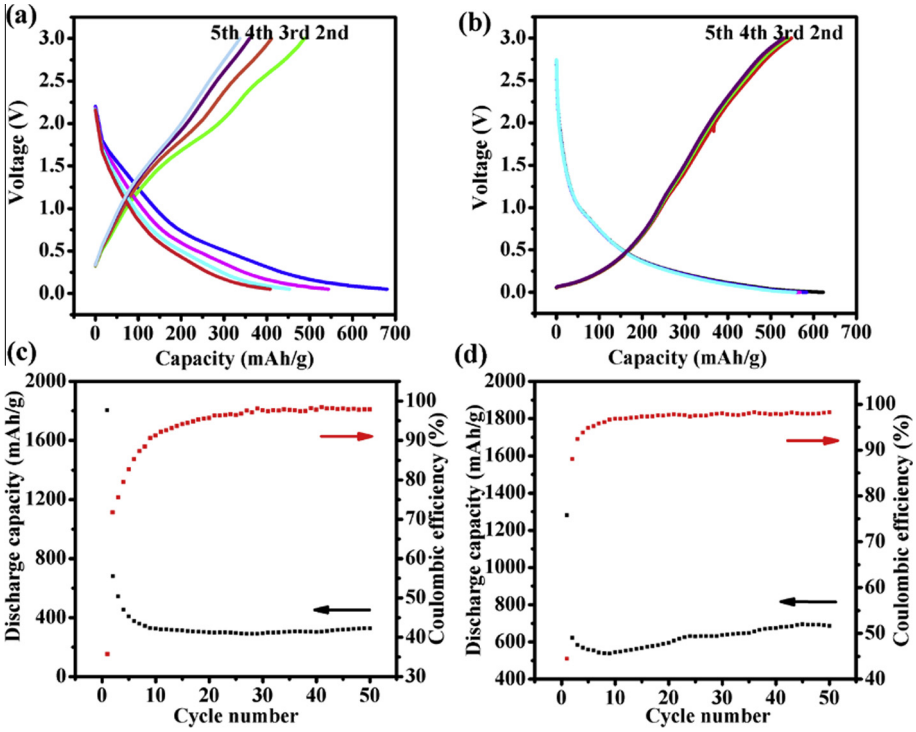

Fig. 7. Galvanostatic charge–discharge profiles of (a) CG and (b) CCG at a current density of 100 mA g^{-1} between 0.01 and 3.00 V (for the second to the fifth cycle); the cycling performance and corresponding coulombic efficiencies of (c) CG (the first coulombic efficiency is 35.7% with the capacity of 328 mAh g^{-1} at the 50th cycle) and (d) CCG (the first coulombic efficiency is 44.5% with the capacity of 685 mAh g^{-1} at the 50th cycle).

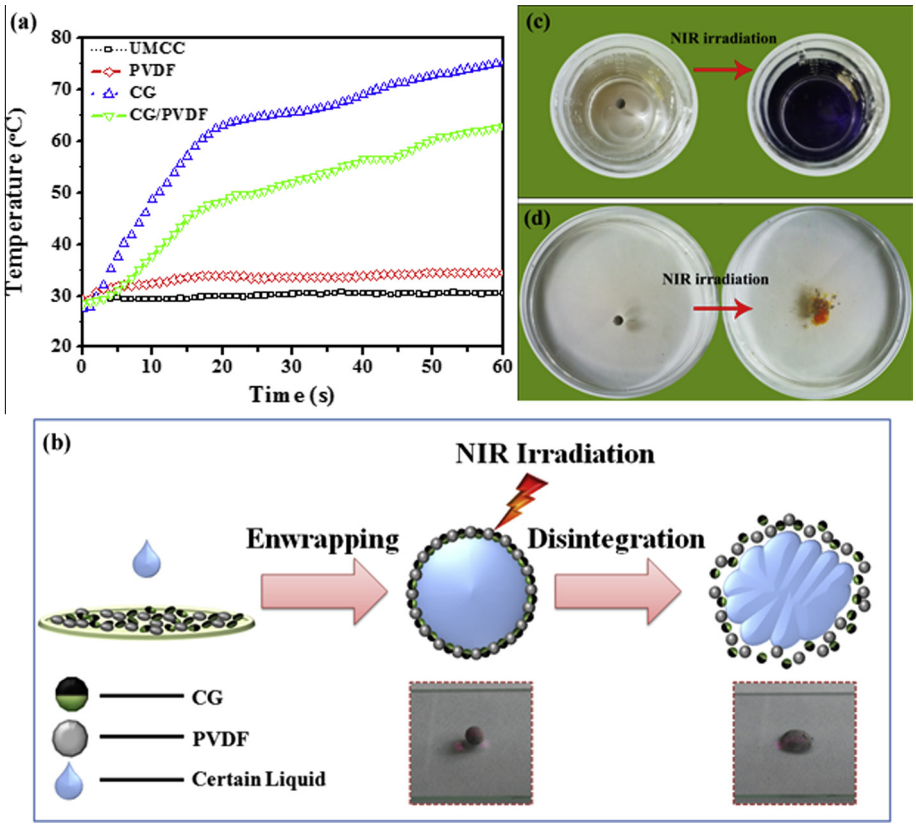

Fig. 8. (a) Temperature profiles of UMCC, PVDF, CG, and CG/PVDF under 808 nm laser irradiation with a power density of 5 W/cm^2. (b) The liquid marble formation and triggered mechanism. Digital photographs of CG/PVDF liquid marble in NIR-triggered chemical reactions: (c) liquid marble containing $FeCl_3$ solution on phenol solution before and after NIR irradiation; (d) liquid marble containing $FeCl_3$ solution on $NaHCO_3$ solution before and after NIR irradiation.

4. Conclusions

CG with a high concentration of 1.12 mg mL^{-1} was successfully prepared by direct liquid-phase exfoliation of graphite in IL-cellulose complexes. It is noteworthy that IL offered a favorable system, in which IL-cellulose complexes acted as an ideal exfoliating agent to obtain few-layer graphene. The composite exhibited attractive electrical properties after carbonization, such as desirable discharge–charge capacities and stable cycling performance as anode materials. Furthermore, CG presented prominent photothermal property with a measured temperature as high as 75 °C after 1 min of irradiation, which was made into a NIR-responsive liquid marble as a trigger for typical chromogenic chemical reactions. CG is a promising candidate for applications in advanced electrochemical and photothermal devices.

Acknowledgements

This work was financially supported by State Key Laboratory of Pulp and Paper Engineering, China (No. 2015C10), the Program for New Century Excellent Talents in University, China (No. NCET-13-0216) and Natural Science Foundation of Guangdong Province, China (No. 2014A030313252).

Appendix A. Supplementary data

Supplementary data associated with this article can be found, in the online version, at http://dx.doi.org/10.1016/j.cej.2016.04.030.

References

[1] Z. Mics, K.-J. Tielrooij, K. Parvez, S.A. Jensen, I. Ivanov, X. Feng, K. Mullen, M. Bonn, D. Turchinovich, Thermodynamic picture of ultrafast charge transport in graphene, Nat. Commun. 6 (2015).
[2] A.A. Balandin, S. Ghosh, W. Bao, I. Calizo, D. Teweldebrhan, F. Miao, C.N. Lau, Superior thermal conductivity of single-layer graphene, Nano Lett. 8 (2008) 902–907.
[3] A.A. Balandin, Thermal properties of graphene and nanostructured carbon materials, Nat. Mater. 10 (2011) 569–581.
[4] C.G. Lee, X.D. Wei, J.W. Kysar, J. Hone, Measurement of the elastic properties and intrinsic strength of monolayer graphene, Science 321 (2008) 385–388.
[5] N.O. Weiss, H. Zhou, L. Liao, Y. Liu, S. Jiang, Y. Huang, X. Duan, Graphene: an emerging electronic material, Adv. Mater. 24 (2012) 5782–5825.
[6] X. Jiang, S. Setodoi, S. Fukumoto, I. Imae, K. Komaguchi, J. Yano, H. Mizota, Y. Harima, An easy one-step electrosynthesis of graphene/polyaniline composites and electrochemical capacitor, Carbon 67 (2014) 662–672.
[7] X. Cao, Y. Shi, W. Shi, G. Lu, X. Huang, Q. Yan, Q. Zhang, H. Zhang, Preparation of novel 3D graphene networks for supercapacitor applications, Small 7 (2011) 3163–3168.
[8] W. Du, S. Qi, B. Zhou, P. Sun, L. Zhu, X. Jiang, A surfactant-free water-processable all-carbon composite and its application to supercapacitor, Electrochim. Acta 146 (2014) 353–358.
[9] Y. Zhang, L. Si, B. Zhou, B. Zhao, Y. Zhu, L. Zhu, X. Jiang, Synthesis of novel graphene oxide/pristine graphene/polyaniline ternary composites and application to supercapacitor, Chem. Eng. J. 288 (2016) 689–700.
[10] H.J. Yoon, J.H. Yang, Z. Zhou, S.S. Yang, M.M.-C. Cheng, Carbon dioxide gas sensor using a graphene sheet, Sens. Actuators, B 157 (2011) 310–313.
[11] R.S. Edwards, K.S. Coleman, Graphene synthesis: relationship to applications, Nanoscale 5 (2013) 38–51.
[12] M.Z. Cai, D. Thorpe, D.H. Adamson, H.C. Schniepp, Methods of graphite exfoliation, J. Mater. Chem. 22 (2012) 24992–25002.
[13] A. O'Neill, U. Khan, P.N. Nirmalraj, J. Boland, J.N. Coleman, Graphene dispersion and exfoliation in low boiling point solvents, J. Phys. Chem. C 115 (2011) 5422–5428.
[14] C.E. Hamilton, J.R. Lomeda, Z. Sun, J.M. Tour, A.R. Barron, High-yield organic dispersions of unfunctionalized graphene, Nano Lett. 9 (2009) 3460–3462.
[15] B. Shen, W. Zhai, D. Lu, J. Wang, W. Zheng, Ultrasonication-assisted direct functionalization of graphene with macromolecules, RSC Adv. 2 (2012) 4713–4719.
[16] M. Petkovic, K.R. Seddon, L.P.N. Rebelo, C. Silva, Pereira, ionic liquids: a pathway to environmental acceptability, Chem. Soc. Rev. 40 (2011) 1383–1403.
[17] L. Crowhurst, P.R. Mawdsley, J.M. Perez-Arlandis, P.A. Salter, T. Welton, Solvent–solute interactions in ionic liquids, Phys. Chem. Chem. Phys. 5 (2003) 2790–2794.
[18] M. Tariq, M.G. Freire, B. Saramago, J.A. Coutinho, J.N.C. Lopes, L.P.N. Rebelo, Surface tension of ionic liquids and ionic liquid solutions, Chem. Soc. Rev. 41 (2012) 829–868.
[19] W.C. Du, X.Q. Jiang, L.H. Zhu, From graphite to graphene: direct liquid-phase exfoliation of graphite to produce single-and few-layered pristine graphene, J. Mater. Chem. A 1 (2013) 10592–10606.
[20] O.A. Battista, P.A. Smith, Microcrystalline cellulose, Ind. Eng. Chem. 54 (1962) 20–29.
[21] L.B. Hu, Y. Cui, Energy and environmental nanotechnology in conductive paper and textiles, Energy Environ. Sci. 5 (2012) 6423–6435.
[22] Y.-R. Rhim, D. Zhang, D.H. Fairbrother, K.A. Wepasnick, K.J. Livi, R.J. Bodnar, D. C. Nagle, Changes in electrical and microstructural properties of microcrystalline cellulose as function of carbonization temperature, Carbon 48 (2010) 1012–1024.
[23] Y. Kaburagi, M. Ohoyama, Y. Yamaguchi, E. Shindou, A. Yoshida, N. Iwashita, N. Yoshizawa, M. Kodama, Acceleration of graphitization on carbon nanofibers prepared from bacteria cellulose dispersed in ethanol, Carbon 50 (2012) 4757–4760.
[24] Y.Y. Li, H.L. Zhu, F. Shen, J.Y. Wan, X.G. Han, J.Q. Dai, H.Q. Dai, L.B. Hu, Highly conductive microfiber of graphene oxide templated carbonization of nanofibrillated cellulose, Adv. Funct. Mater. 24 (2014) 7366–7372.
[25] M.C. Wu, A.R. Deokar, J.H. Liao, P.Y. Shih, Y.C. Ling, Graphene-based photothermal agent for rapid and effective killing of bacteria, ACS Nano 7 (2013) 1281–1290.
[26] Y.Z. Ling, X.Y. Li, S.W. Zhou, X.Y. Wang, R.C. Sun, Multifunctional cellulosic paper based on quaternized chitosan and gold nanoparticle-reduced graphene oxide via electrostatic self-assembly, J. Mater. Chem. A (2015) 7422–7428.
[27] P. McEleney, G.M. Walker, I.A. Larmour, S.E.J. Bell, Liquid marble formation using hydrophobic powders, Chem. Eng. J. 147 (2009) 373–382.
[28] K. Nakai, H. Nakagawa, K. Kuroda, S. Fujii, Y. Nakamura, S. Yusa, Near-infrared-responsive liquid marbles stabilized with carbon nanotubes, Chem. Lett. 42 (2013) 719–721.
[29] D. Li, M.B. Müller, S. Gilje, R.B. Kaner, G.G. Wallace, Processable aqueous dispersions of graphene nanosheets, Nat. Nanotechnol. 3 (2008) 101–105.
[30] D.F. Swinehart, The Beer–Lambert law, J. Chem. Educ. 39 (1962) 333.
[31] X.Q. Wang, P.F. Fulvio, G.A. Baker, G.M. Veith, R.R. Unocic, S.M. Mahurin, M.F. Chi, S. Dai, Direct exfoliation of natural graphite into micrometre size few layers graphene sheets using ionic liquids, Chem. Commun. 46 (2010) 4487–4489.
[32] D. Nuvoli, L. Valentini, V. Alzari, S. Scognamillo, S.B. Bon, M. Piccinini, J. Illescas, A. Mariani, High concentration few-layer graphene sheets obtained by liquid phase exfoliation of graphite in ionic liquid, J. Mater. Chem. 21 (2011) 3428–3431.
[33] C.N.R. Rao, A.K. Sood, K.S. Subrahmanyam, A. Govindaraj, Graphene: the new two-dimensional nanomaterial, Angew. Chem. Int. Ed. 48 (2009) 7752–7777.
[34] Q.Z. Cheng, S.Q. Wang, Q.Y. Han, Novel process for isolating fibrils from cellulose fibers by high-intensity ultrasonication. II. Fibril characterization, J. Appl. Polym. Sci. 115 (2010) 2756–2762.
[35] M.H. Jin, T.H. Kim, S.C. Lim, D.L. Duong, H.J. Shin, Y.W. Jo, H.K. Jeong, J. Chang, S. S. Xie, Y.H. Lee, Facile physical route to highly crystalline graphene, Adv. Funct. Mater. 21 (2011) 3496–3501.
[36] A.C. Ferrari, J.C. Meyer, V. Scardaci, C. Casiraghi, M. Lazzeri, F. Mauri, S. Piscanec, D. Jiang, K.S. Novoselov, S. Roth, Raman spectrum of graphene and graphene layers, Phys. Rev. Lett. 97 (2006) 187401.
[37] A.C. Ferrari, Raman spectroscopy of graphene and graphite: disorder, electron–phonon coupling, doping and nonadiabatic effects, Solid State Commun. 143 (2007) 47–57.
[38] K.N. Kudin, B. Ozbas, H.C. Schniepp, R.K. Prud'Homme, I.A. Aksay, R. Car, Raman spectra of graphite oxide and functionalized graphene sheets, Nano Lett. 8 (2008) 36–41.
[39] Y.Y. Feng, X.Q. Zhang, Y.T. Shen, K. Yoshino, W. Feng, A mechanically strong, flexible and conductive film based on bacterial cellulose/graphene nanocomposite, Carbohydr. Polym. 87 (2012) 644–649.
[40] Y. Maréchal, H. Chanzy, The hydrogen bond network in I_β cellulose as observed by infrared spectrometry, J. Mol. Struct. 523 (2000) 183–196.
[41] J. Łojewska, P. Miśkowiec, T. Łojewski, L. Proniewicz, Cellulose oxidative and hydrolytic degradation: in situ FTIR approach, Polym. Degrad. Stab. 88 (2005) 512–520.
[42] Z. Lin, G. Waller, Y. Liu, M. Liu, C.P. Wong, Facile synthesis of nitrogen-doped graphene via pyrolysis of graphene oxide and urea, and its electrocatalytic activity toward the oxygen-reduction reaction, Adv. Energy Mater. 2 (2012) 884–888.
[43] M. Belgacem, G. Czeremuszkin, S. Sapieha, A. Gandini, Surface characterization of cellulose fibres by XPS and inverse gas chromatography, Cellulose 2 (1995) 145–157.
[44] Z.F. Wang, J.Q. Wang, Z.P. Li, P.W. Gong, X.H. Liu, L.B. Zhang, J.F. Ren, H.G. Wang, S.R. Yang, Synthesis of fluorinated graphene with tunable degree of fluorination, Carbon 50 (2012) 5403–5410.
[45] J.Y. Liu, H.Y. Chang, Q.D. Truong, Y.C. Ling, Synthesis of nitrogen-doped graphene by pyrolysis of ionic-liquid-functionalized graphene, J. Mater. Chem. C 1 (2013) 1713–1716.
[46] R. Bari, G. Tamas, F. Irin, A.J.A. Aquino, M.J. Green, E.L. Quitevis, Direct exfoliation of graphene in ionic liquids with aromatic groups, Colloids Surf. A 463 (2014) 63–69.
[47] H. Wang, G. Gurau, R.D. Rogers, Ionic liquid processing of cellulose, Chem. Soc. Rev. 41 (2012) 1519–1537.

[48] W. Li, J. Yue, S. Liu, Preparation of nanocrystalline cellulose via ultrasound and its reinforcement capability for poly (vinyl alcohol) composites, Ultrason. Sonochem. 19 (2012) 479–485.
[49] D. Philp, J.M. Robinson, A computational investigation of cooperativity in weakly hydrogen-bonded assemblies, J. Chem. Soc. Perkin Trans. 2 (1998) 1643–1650.
[50] J.-M. Malho, P.i. Laaksonen, A. Walther, O. Ikkala, M.B. Linder, Facile method for stiff, tough, and strong nanocomposites by direct exfoliation of multilayered graphene into native nanocellulose matrix, Biomacromolecules 13 (2012) 1093–1099.
[51] V. Channu, R. Bobba, R. Holze, Graphite and graphene oxide electrodes for lithium ion batteries, Colloids Surf. A 436 (2013) 245–251.
[52] X. Huang, Z. Zeng, Z. Fan, J. Liu, H. Zhang, Graphene-based electrodes, Adv. Mater. 24 (2012) 5979–6004.